Correspondence to:
Y. Mau,
yair.mau@mail.huji.ac.il

Soil Degradation Risks Assessed by the SOTE Model for Salinity and Sodicity

Isaac Kramer[1] and **Yair Mau[1]**

[1]Department of Soil and Water Sciences, The Robert H. Smith Faculty of Agriculture, Food and Environment, The Hebrew University of Jerusalem, Rehovot, Israel

Abstract Soil salinity and sodicity are serious environmental hazards, with the potential to limit agricultural production and cause destructive soil degradation. These concerns are especially high in dry areas, which often rely on saline and sodic irrigation water to support agriculture. To assess long-term soil degradation risk, we introduce the Salt of the Earth (SOTE) model, which describes the dynamics of soil water content, salinity, and sodicity, as driven by irrigation and rainfall. The SOTE model incorporates how changes in salinity and sodicity affect saturated soil hydraulic conductivity, K_s, on a soil-specific basis. The model was successfully validated against results from a multiyear lysimeter experiment involving different irrigation water qualities and precipitation. We evaluated the impact of shorter rainy seasons on the dynamics of soil degradation in a Mediterranean climate. Critical degradation risk, indicated by reductions in K_s greater than 20%, increased from 0% to 3% when the rainy season was shortened from 130 to 80 days. Alarmingly, when irreversible degradation is allowed for, overall risk increases to 68%. Assessing the effect of irrigation water on different soils textures, we found that while greater clay fractions are usually more susceptible to dispersion, accurate risk assessment hinges on soil water dynamics. SOTE is amenable to large-ensemble simulations of stochastic climatic conditions, for which trends in the statistics of salinization and soil degradation can be identified. As such, SOTE can be a useful land management tool, allowing planners to understand the risk of long-term soil degradation given irrigation practices, soil qualities, and climate conditions.

1. Introduction

Soil salinity and sodicity present major challenges to agricultural production, including the risk of soil degradation. Saline soils are defined by the presence of various electrolytic mineral solutes in concentrations that decrease crop yields (FAO & ITPS, 2015; Hillel, 2000; Läuchli & Grattan, 2011). Soil sodicity refers specifically to the concentration of sodium ions in soil and soil water. High relative sodium concentrations, when combined with relatively low salinity, can lead to soil degradation, limiting the movement of air and water within the soil (FAO & ITPS, 2015; Hillel, 2000; Läuchli & Grattan, 2011). Worldwide, approximately 23% of all cultivated lands are considered saline and 37% sodic, leading to significant economic losses and risk to future agriculture production (Wallender & Tanji, 2011).

Arid and semiarid regions, which require irrigation to sustain agricultural production, are especially vulnerable to the threats presented by soil salinity and sodicity (Chesworth, 2008; FAO & ITPS, 2015). Limited water resources in these regions encourage the use of low-quality waters with high salt and sodium concentrations (Hillel, 2000). In contrast to humid regions, the annual precipitation received in dry areas often fails to flush salts from the soil's root zone (Chesworth, 2008; Lado et al., 2012). Even when adequate leaching occurs, irrigation with saline water can cause groundwater pollution (El-Din et al., 1987; Lado et al., 2012). Anticipated increases in water stress, together with expected changes in rainfall patterns resulting from climate change, have the potential to further exacerbate the dangers posed by soil salinity and sodicity (Stocker, 2014; The Water Resources Group, 2012; Vereecken et al., 2016).

While irrigation with low-quality water can support agricultural production in areas that would otherwise be uncompetitive (Raveh & Ben-Gal, 2016), reclaiming degraded soils is resource expensive and time consuming (Tanji & Deverel, 1984). At present, only crude guidelines exist for estimating how a soil will respond to the application of saline and sodic waters. More accurate models can increase our ability to determine the

risk of soil degradation, including how variations in soil type and climate conditions may affect the probability of degradation. As tools for smarter decision making, improved models can allow us to maximize the use of marginal quality lands while simultaneously avoiding soil degradation.

Existing models are not optimally suited to analyzing how environmental conditions and irrigation practices affect soils *over the long term*. The majority are detail-heavy and require fully solving Richards equation for unsaturated water flow and advection diffusion equations for solute transport (Ahuja et al., 2000; Hutson & Wagenet, 1989; Kroes et al., 2009; Russo, 1989; Šimůnek & Suarez, 1997). In addition to being computationally demanding, these models require several soil-specific parameters as inputs and can fail under certain soil conditions, such as a fast wetting rate (Farthing & Ogden, 2017; Short et al., 1995; Tocci et al., 1997). The complicated nature of these models, which often includes numerous processes secondary to soil salinity, obscures our ability to analyze the relationships between variables and output, especially over the long term.

In this paper we introduce the SOTE model (Salt of the Earth), which describes the coupled dynamics of soil water, salinity, and sodicity. Our goal in developing this model is to understand how irrigation practices and stochastic climatic conditions interplay with major soil feedbacks, potentially leading to long-term soil degradation. As such, SOTE contributes to the growing interest in the stochastic nature of water and salt dynamics (Mau & Porporato, 2015, 2016; Mau et al., 2014; Perri et al., 2018; Shah et al., 2011; Suweis et al., 2010; van der Zee et al., 2014; Vico & Porporato, 2010). The SOTE model is both the equations developed in this paper and their implementation as an open-source Python code. This model expands the scope of previous modeling efforts (Mau & Porporato, 2015,2016), including explicit treatment of soil water dynamics and the effect of soil salinity and sodicity on saturated hydraulic conductivity, K_s. In contrast to van der Zee et al. (2014), the equations we develop consider input and outputs of salt from irrigation—particularly important in dryland and arid regions—and plant uptake, in addition to groundwater and precipitation. SOTE is also unique in its implementation of the complete soil-specific function for K_s introduced by Ezlit et al. (2013).

Our objective in designing SOTE is the optimal study of the long-term dynamics of salinity and sodicity and how these contribute to the risk of soil degradation. In contrast to more demanding numerical models, SOTE seeks to use efficient equations to model the main processes that drive salinity and sodicity. At the same time, it aims to take an advanced approach to modeling the feedbacks associated with these processes, explicitly considering soil-specific properties. This combination makes SOTE a novel tool for assessing the risk of soil degradation under different irrigation and climate regimes.

We begin with the development of the SOTE model (section 2). We then validate SOTE against results from a multiyear lysimeter experiment and compare its performance with simulations produced by the Hydrus software package (section 3). Finally, we investigate soil degradation risks resulting from changes in seasonal rainfall patterns, different soil types, and irrigation water quality (section 4).

2. Model Development

The SOTE model aims to study the long-term dynamics of soil water content, salinity, and sodicity, as driven by irrigation practices and climatic conditions. The model specifically focuses on how these processes can cause soil degradation through reductions in soil hydraulic conductivity. We introduce three state variables to characterize the dynamics of the system: relative water content, soil salinity, and soil sodicity. We define relative soil water content, s (dimensionless), as the fraction of the soil's pore volume containing water (i.e., volumetric water content θ divided by porosity n). We define soil salinity, C_s, as the electrolyte concentration of salts in the soil water (mmol$_c$/L). We define soil sodicity, E_x (dimensionless), as the fraction of sodium ions in the soil's exchange complex (i.e., the Exchangeable Sodium Percentage, ESP, reported as a fraction). The dynamics of the state variables are described by coupled, nonlinear ordinary differential equations based on mass balance for water and salts. A graphic overview of the SOTE model is included in Figure 1, while Table 1 defines the variables and parameters used throughout this paper.

Changes to soil water content are driven by inputs of irrigation (I), precipitation (P), and groundwater (U) and losses from evapotranspiration (ET), leakage (L), and runoff (Q). Irrigation can be considered as either a constant rate (e.g., mm/day), triggered by soil water content, or a time-dependent process (e.g., weekly flood irrigation). Random precipitation events are modeled as a marked Poisson process (Rodriguez-Iturbe & Porporato, 2004), with mean interarrival time λ^{-1} and rainfall depth drawn from an
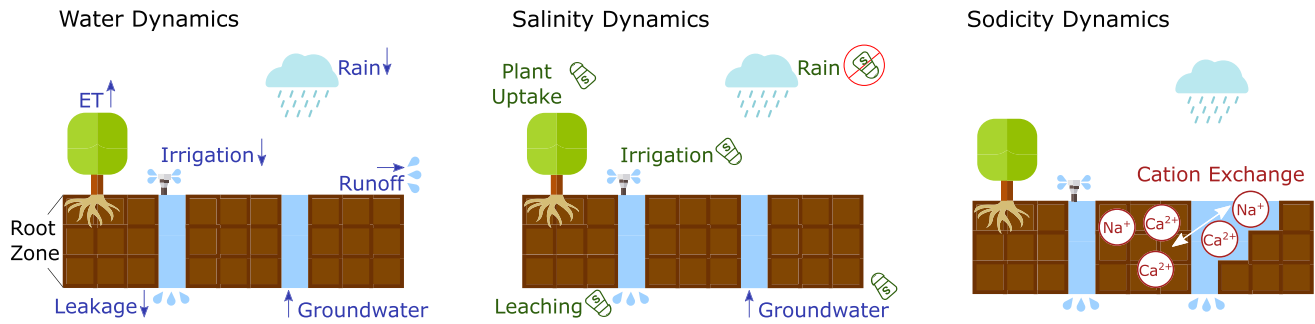
Figure 1. The SOTE model focuses on the dynamics of soil water content, salinity, and sodicity in the root zone, as driven by irrigation practices and climatic conditions. Each panel indicates one of the major processes considered in the dynamics of the state variables.

exponential distribution with mean α. Actual evapotranspiration and leakage rates depend on soil water content and maximum potential evapotranspiration. Precipitation, evapotranspiration, and irrigation rates can be defined to vary seasonally. Our model also accepts irrigation, precipitation, and evapotranspiration rates drawn from measured time series. In this paper, we only draw values from a measured time series when validating the model. Runoff is generated through saturation excess, when relative soil water content reaches $s = 1$, and through infiltration excess, when water input rates ($I + P$) are higher than soil hydraulic conductivity. Groundwater can be accounted for using the modeling technique presented by Vervoort and van der Zee (2008), wherein the flux of groundwater is dependent on soil water content, hydraulic functions, and distance from the root zone to the groundwater.

As water enters and exits the system, it causes changes in both the salinity of the water in the root zone and in the sodicity of the soil. These changes are driven by the different chemical composition (total solute concentration and sodium fraction) of the different input waters. Irrigation water is the major source of salt inputs considered by SOTE, and leaching is the primary removal mechanism, but input from groundwater and output from plant uptake are also allowed for. As salt cations pass through the system, they interact with the cations adsorbed to the soil exchange complex. Due to our focus on long-term processes, we consider the soil solution and exchange complex to be in equilibrium, as described by the Gapon equation.

The most important feedback considered by SOTE is the effect the chemical composition of the soil water has on soil hydraulic conductivity. Here, we incorporate the empirical model developed by Ezlit et al. (2013), which describes how the fraction of sodium cations in a soil's exchange complex, coupled with overall salinity, can lead to a breakdown in soil structure and thereby a reduction in saturated soil hydraulic conductivity, $K_s(C_s, E_x)$.

A number of important assumptions are made in constructing the SOTE model. There are no explicit spatial dimensions: Soil water and salt are averaged in the horizontal directions and over the rooting depth, Z_r (mm). The soil solute concentration and its sodium fraction are well mixed within the rooting depth, so the drainage water reflects the composition of the soil solute. In our simulations, we focus on input of salts from irrigation and ignore any salts from precipitation, but the equations are written such that the chemical composition of the rain and groundwater is also considered. Finally, we restrict our focus to only two cations: Na^+ and Ca^{2+}. This allows us to simplify the equations describing the chemical balance of the system and to concentrate on the distinctions between divalent cations, known to support the formation of soil aggregates, and monovalent cations, related to soil degradation (Hillel, 1998).

2.1. Soil Water Dynamics

The balance equation for the relative soil water content s is

$$nZ_r \frac{ds}{dt} = P(t) + I(t) + U(s) - ET(s) - L(s) - Q(s). \tag{1}$$

The water inputs are precipitation (P), irrigation (I), and groundwater (U), whereas outputs are evapotranspiration (ET), leakage to deeper soil layers (L), and runoff (Q), all reported in mm/day. Leakage losses follow a power law of s (Clapp & Hornberger, 1978), while evapotranspiration is modeled following Laio et al. (2001). A brief description of their functional forms is found in the supporting information (Text S1).

Table 1
Definition of All Symbols Used Throughout This Paper

Symbol	Units	Description
C	$mmol_c/L$	Electrolyte concentration
c	—	Soil-specific constant used in calculating leakage rate
CEC	$mmol_c/kg$	Cation exchange capacity
E	—	Sodium fraction
ESP	—	Exchangeable sodium %
ESR	—	Exchangeable sodium ratio
ET	mm/day	Evapotranspiration rate
ET_{max}	mm/day	Maximal evapotranspiration rate
ET_w	mm/day	Evapotranspiration rate at wilting point
I	mm/day	Irrigation rate
K_g	$(mmol_c/L)^{-1/2}$	Gapon selectivity coefficient
K_s	mm/day	Saturated hydraulic conductivity
K_{CT}	mm/day	Critical threshold in K_s
L	mm/day	Leakage rate
M	kg/m^2	Dry soil mass
n	—	Soil porosity
P	mm/day	Precipitation rate
Q	mm/day	Runoff rate
q	$mmol_c/L/m^2$	Salt content
s	—	Relative soil water content (θ/n)
SAR	$(mmol_c/L)^{1/2}$	Sodium adsorption ratio
T	mm/day	Plant uptake rate
U	mm/day	Groundwater uptake rate
w	L/m^2	Volumetric soil water
Z_r	mm	Rooting depth
λ^{-1}	—	Mean interarrival time
α	mm	Mean Rainfall depth
i subscript	—	Irrigation water
r subscript	—	Rain water
s subscript	—	Soil water
u subscript	—	Groundwater
x subscript	—	Exchange complex
0 subscript	—	Initial condition

In the following sections it is often convenient to express the water content w in terms of water volume per unit area. This can be done by noting that $w = nZ_r s$, which has units of L/m^2.

2.2. Salinity Dynamics

To develop an equation for C_s, the concentration of salts in the soil water, we begin by defining the mass balance for q_s, the total salt content per square meter ($mmol_c/m^2$) in the soil water:

$$\frac{dq_s}{dt} = IC_i + PC_r + U(s)C_u - L(s)C_s - \beta T(s)C_s, \tag{2}$$

where the subscripts i, r, u, and s refer to the irrigation water, rain, groundwater, and soil water, respectively. In doing so, we expand on Mau and Porporato (2015), which considered only irrigation and leakage. The first three terms represent salt input from irrigation, rain, and groundwater. The last two terms denote salt losses through leaching to deeper soil layers or groundwater and plant uptake (T), where β relates the concentration of the soil water with that of plant uptake. Formally, salt content, q_s, is our second state variable,

for which we have a differential equation and not concentration, C_s. However, given that $C_s = q_s/w$, we can calculate C_s using the results from Equations 2 and 1.

2.3. Sodicity Dynamics

We develop an equation for E_x (i.e., ESP/100), the fraction of sodium ions in the soil's exchange complex, using the principles applied to find mass balance equations for water and salinity. As before, we build on the work of Mau and Porporato (2015). The input and output of sodium from the system are governed by the same processes that determine the change in total salt content, and therefore, we can write the balance equation for sodium ions as follows:

$$\frac{dq^{\mathrm{Na^+}}}{dt} = IC_i E_i^{\mathrm{Na^+}} + PC_r E_r^{\mathrm{Na^+}} + U_s(s)C_u E_u^{\mathrm{Na^+}} - L_s(s)C_s E_s^{\mathrm{Na^+}} - T_s(s)C_s E_s^{\mathrm{Na^+}}, \tag{3}$$

where $q^{\mathrm{Na^+}}$ is the total sodium content in the system and $E_i^{\mathrm{Na^+}}$, $E_r^{\mathrm{Na^+}}$, $E_u^{\mathrm{Na^+}}$, and $E_s^{\mathrm{Na^+}}$ are the fraction of sodium cations in irrigation, rain, groundwater, and soil solution, respectively. The total mass of sodium is the sum of the sodium ions in the soil water ($q_s^{\mathrm{Na^+}}$) and the sodium ions adsorbed to the soil exchange complex ($q_x^{\mathrm{Na^+}}$), such that

$$q^{\mathrm{Na^+}} = q_s^{\mathrm{Na^+}} + q_x^{\mathrm{Na^+}}. \tag{4}$$

Recognizing that the sodium in the exchange complex is given by $q_x^{\mathrm{Na^+}} = \mathrm{CEC} \cdot M \cdot E_x$ (where CEC is the Cation Exchange Capacity and M is the mass of dry soil contained in a unit area of soil with depth Z_r), we substitute Equation 4 into Equation 3, thus obtaining a differential equation for E_x. The complete equation and its derivation are contained in Text S2. In deriving the differential equation for E_x, we utilize the Gapon equation to develop an exchange isotherm to describe the exchange of cations between the soil's exchange complex and the water in the soil's root zone. The Gapon equation and the resulting isotherm are described in Text S3. Any alternative exchange isotherm (e.g., the Vanselow equation) could be used in place of the Gapon.

2.4. Saturated Hydraulic Conductivity

The dependence of saturated hydraulic conductivity on salinity and sodicity, $K_s(C_s, E_x)$, lies at the heart of the soil degradation process considered in this paper. It comes into play in the leakage term, in Equation 1, for the soil water dynamics:

$$L(s, C_s, E_x) = K_s(C_s, E_x)s^c, \tag{5}$$

where c is a soil-specific constant. To model this feedback, we incorporate the disaggregation model introduced by Ezlit et al. (2013). In contrast to McNeal (1968), the model presented by Ezlit et al. (2013) includes soil-specific parameters and the boundary between clay flocculation and dispersion. The parameters introduced by Ezlit et al. (2013) allow for the examination of how different soils respond to changing salinity and sodicity levels, enhancing our ability to link salinity and sodicity dynamics with degradation risks on a soil-specific basis. The novelty of the Ezlit et al. (2013) model is demonstrated in Equation 2, which applies the model to demonstrate how three typical soils can experience different declines in hydraulic conductivity at the same salinity and sodicity levels. The higher the clay content, the more sensitive the soil to reductions in K_s. However, as will be shown in section 4, this does not necessarily mean that clayey soil is more prone to degradation than other soils, for the same irrigation regime and climatic conditions. Validation of the Ezlit et al. (2013) model has shown that it is able to effectively predict reductions in hydraulic conductivity in a wide variety of soils as a result of saline and sodic water (Dang et al., 2018), though it does not consider the effects of other factors such as pH (Ali et al., 2019). A short overview of the Ezlit et al. (2013) model is included in Text S4.

3. Validation

In this section we validate SOTE against measured results and model simulations. We focus here on the validation of the salinity and sodicity functions, while results from the validation of the soil water content are included in Text S6.
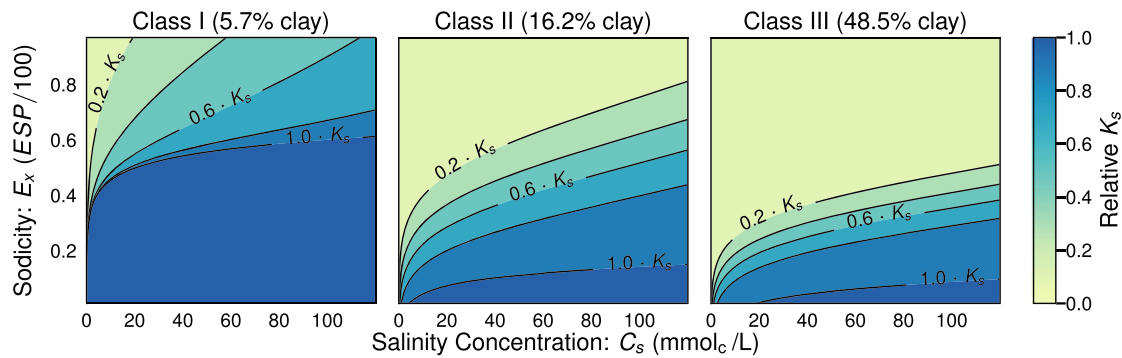
Figure 2. Integration of the (Ezlit et al., 2013) model allows for consideration of soil-specific changes in hydraulic conductivity resulting from the dynamics of salinity and sodicity. Panels show the dependence of relative K_s in the salinity-sodicity space, for soils with increasing clay content.

3.1. Methodology

We validated SOTE as a tool for studying the long-term dynamics of salinity and sodicity against experimental data from Gonçalves et al. (2006). Conducted in southern Portugal, this 4-year study measured soil salinity and sodicity in lysimeters. During the summer (dry season), irrigation waters of increasing levels of salinity and sodicity were applied to three lysimeters (A, B, and C). The salinity (C_i), sodicity fraction (E_i), and SAR of the irrigation waters are shown in Table 2. During the winter (rainy season), the lysimeters were exposed to precipitation. The salinity of the soil solution was measured on an approximately weekly basis at four soil depths, 10, 30, 50, and 70 cm. Soil ESP was measured at five soil depths (10, 30, 50, 70, and 90 cm) at the beginning of the measurement period, at the end of each irrigation season, and at the end of each rainy season. The initial soil physical and chemical properties needed to run the SOTE model are shown in Table S3. These values are as reported in Gonçalves et al. (2006), with the exception of the Gapon selectivity coefficient, which is defined differently in our model. An explanation of the conversion is contained in Text S5. Inputs for evapotranspiration and precipitation were based on data from a meteorological station 10 m from the experimental site, provided by the study's authors. We note that because the experiments were conducted using lysimeters, our validation does not include a groundwater term and assumes free drainage.

Based on the textural composition of the soil used in the experiment, we estimated values for the parameters related to water losses from the soil (i.e., evapotranspiration and leakage) according to the typical values included in Laio et al. (2001). Likewise, because of the relative clay content of the soil (11% by mass), we used the Class II parameter values reported in Ezlit et al. (2013) when modeling the dependence of saturated hydraulic conductivity on the system's salinity and sodicity. These two sets of parameters are shown in Table S4.

In performing our validation, we also compared SOTE to results produced by the Hydrus 1-D software package (Šimůnek et al., 2013). The results of the Hydrus simulations, including discussion of the Hydrus set-up, were included in Gonçalves et al. (2006), but we note here that the soil hydraulic parameters were optimized according the van Genuchten-Mualem equations and soil water retention data. All of the results used in our

Table 2
Salinity and Sodicity of Irrigation Waters Used During 4-Year Lysimeter Experiment Conducted by Gonçalves et al. (2006)

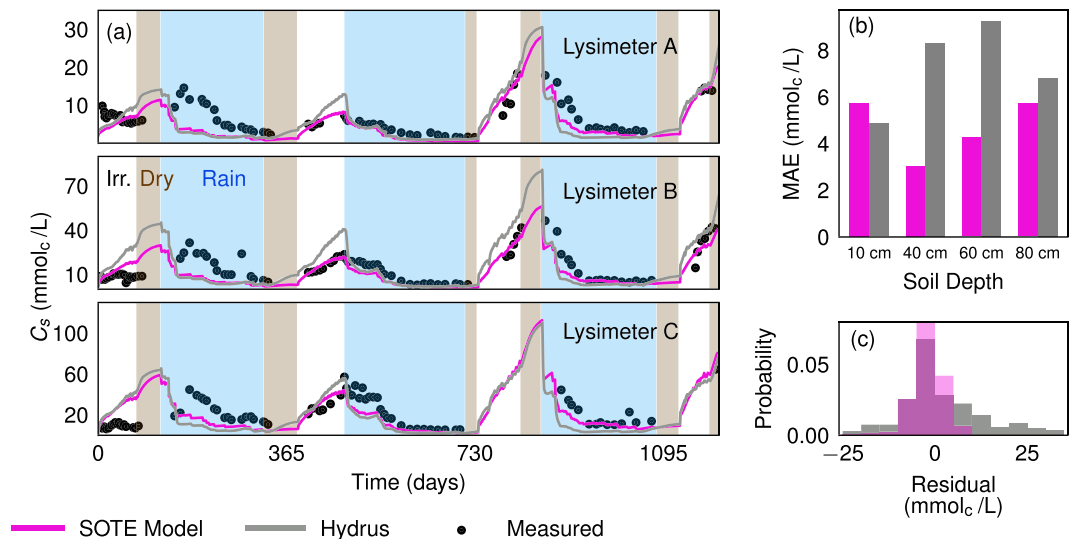| Lysimeter	Salinity (C_i, $mmol_c$/L)	Sodicity (E_i)	SAR
Irrigation Regime I (Years 1 and 2)			
A	3.0	0.33	1.0
B	8.0	0.52	3.0
C	16.0	0.64	6.0
Irrigation Regime II (Years 3 and 4)			
A	8.0	0.31	1.5
B	16.0	0.41	3.0
C	32.0	0.52	6.0

Figure 3. Validation of SOTE simulations for soil salinity (C_s) against measured values and Hydrus. (a) Measured and simulated C_s in lysimeters A, B, and C. The blue shade in the background denotes the rainy season, the white shade denotes irrigation season, and brown shade denotes periods between irrigation and rain. (b) Mean absolute error for SOTE and Hydrus compared to the measured results. (c) Distribution of residuals for SOTE and Hydrus.

validation—including the measured results and Hydrus and SOTE output—are included in the online repository for this paper (see section A1). One important distinction between Hydrus and SOTE is their respective treatments of the soil's vertical profile. Hydrus models flow within the soil profile and can be parameterized to reflect different soil layers. SOTE, on the other hand, is a lumped model that considers average soil conditions and inputs and outputs to the soil system as a whole. When running SOTE with a given soil depth Z_r, we compare our results to all measurements and Hydrus simulations above this soil depth. Specifically, in the validation that follows SOTE simulations with a root zone of 40 cm were compared to averaged Hydrus and measured results, respectively, from 10 and 30 cm. Comparison of the measured and modeled results at other soil depths (plots not included) was done using the same methodology and produced results with similar levels of accuracy.

3.2. Salinity Validation

Figure 3a shows the measured soil solution salinity (C_s, black circles) compared to SOTE and Hydrus simulations (pink and gray curves, respectively). The modeled results capture the main trends in the measurements: a rise in C_s during each irrigation season and leaching of nearly all the salts during the subsequent rainy seasons. The largest peaks in C_s are seen in Lysimeter C, which received the most saline irrigation water. In all lysimeters, the values of C_s are largest in the third and fourth years of the study, when the salinity of the irrigation water was increased. As noted in Gonçalves et al. (2006), missing data toward the end of the dry seasons occasionally prevent the measured results from capturing the peaks in C_s shown in the simulations. The missing data are attributed to soil water contents that were too low to reliably measure salinity, resulting from gaps between the final irrigation treatment and the first precipitation event (Gonçalves et al., 2006).

Figure 3b shows the mean absolute error (MAE) for the simulated C_s values produced by SOTE and Hydrus compared to the measured C_s values. The MAE measures the average of the absolute residuals or the distances between the measured and modeled results. SOTE attained lower MAE than Hydrus, except for depth 10 cm, for which both had comparable performance. Calculation of the root-mean-square error (RMSE) also shows lower values for SOTE, except at 10 cm, for which SOTE and Hydrus are equal (see Text S6). This reinforces our claim that SOTE, despite its relative simplicity, captures the general trends in salinity. The distribution of the residuals for both SOTE and Hydrus is also comparable (Figure 3c). Both are centered about zero (similar accuracy) and bell shaped, with SOTE's distribution narrower (higher precision).

3.3. Sodicity Validation

Figure 4a shows the measured sodicity (E_x) against SOTE and Hydrus simulations. In Lysimeters B and C, both SOTE and the measured results show a rise in E_x during the irrigation season and steady or slightly
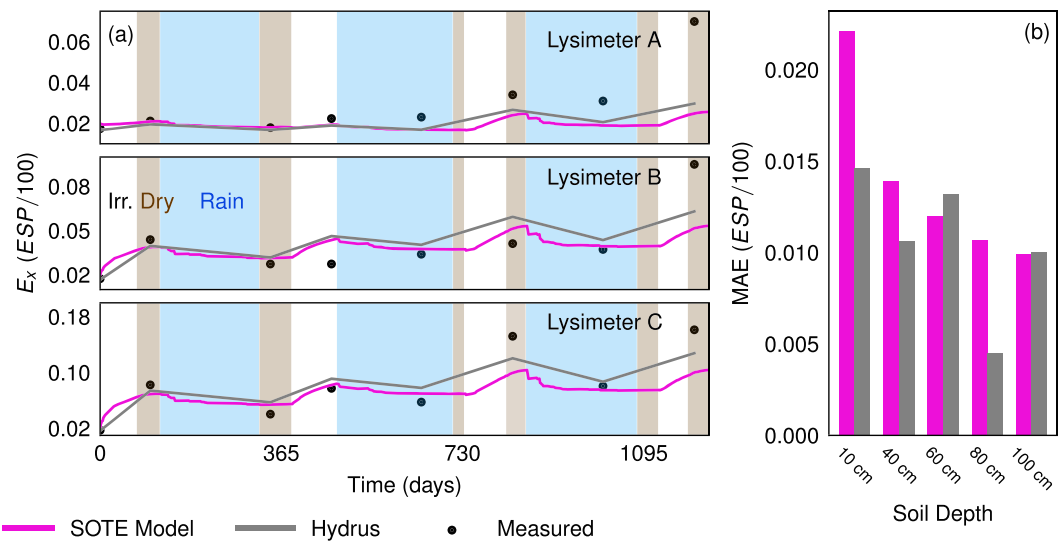
Figure 4. Validation of the SOTE model simulations for soil sodicity (E_x) against the measured values and Hydrus. (a) Measured and simulated E_x in lysimeters A, B, and C. (b) Mean absolute error for SOTE and Hydrus compared to the measured results.

declining values during the rainy season. This trend is also evident in Lysimeter A during Years 3 and 4 of the study. The irrigation water used in Lysimeter A was the least saline and sodic, and the low E_x values in both the measured and modeled results reflect this. Likewise, the increase in E_x is most pronounced in Lysimeter C, which received irrigation water with the highest SAR. Both Hydrus and SOTE significantly underpredict the final measured sodicity value, likely due to an over estimation of the leaching in the preceding rainy season. Given the relatively small residuals for all other points, however, we argue that SOTE and Hydrus provide satisfactory fits to the measured data.

Figure 4b shows the MAE for the simulated values of E_x produced by SOTE and Hydrus compared to the measured sodicity. The residuals produced by the SOTE model are generally larger than those produced by Hydrus, but this difference is not statistically significant due to the low number of measured values (only 8 points are available throughout a 4-year experiment). Calculation of the RMSE shows a similar level of error for SOTE and Hydrus (see Text S6). Again, the size of the MAE and RMSE is affected by the large residual in both SOTE and Hydrus at the final measurement point. Even the largest MAE, however, that for SOTE at 10 cm, is just over 0.02. In all other cases, the MAE is less than 0.015, which we believe is an acceptable degree of error.

3.4. Comparison Between SOTE and Hydrus

SOTE and Hydrus compare similarly well to the measured data. The two models, however, differ greatly in their structure and, as a result of this, their relative strengths. In contrast to Hydrus, SOTE does not require solving the Richards equation, considers only averaged conditions within a soil profile, and focuses on only two cations. The detailed nature of Hydrus may give it an advantage when, for example, conducting research on questions involving short-term processes, complex chemistry, or flow through a layered soil profile. The simplicity of SOTE's equations, however, makes it a unique tool for researching long-term processes. The easy ability to conduct thousands of simulations with stochastic rainfall makes SOTE ideally suited for studying, for instance, the effect of changing climate conditions on soil degradation, as we do in the next section.

4. Model Applications

4.1. General Design of Simulations

In this section we use stochastic simulations to study the role of soil type, irrigation practices, and climate change on soil degradation in dryland and arid regions. Because rainfall is generally seasonal in these areas, we designed our simulations so that rainfall was possible during only a fraction of the year. Rainfall during this period was treated as a marked Poisson process, as described in section 2. All of our simulations
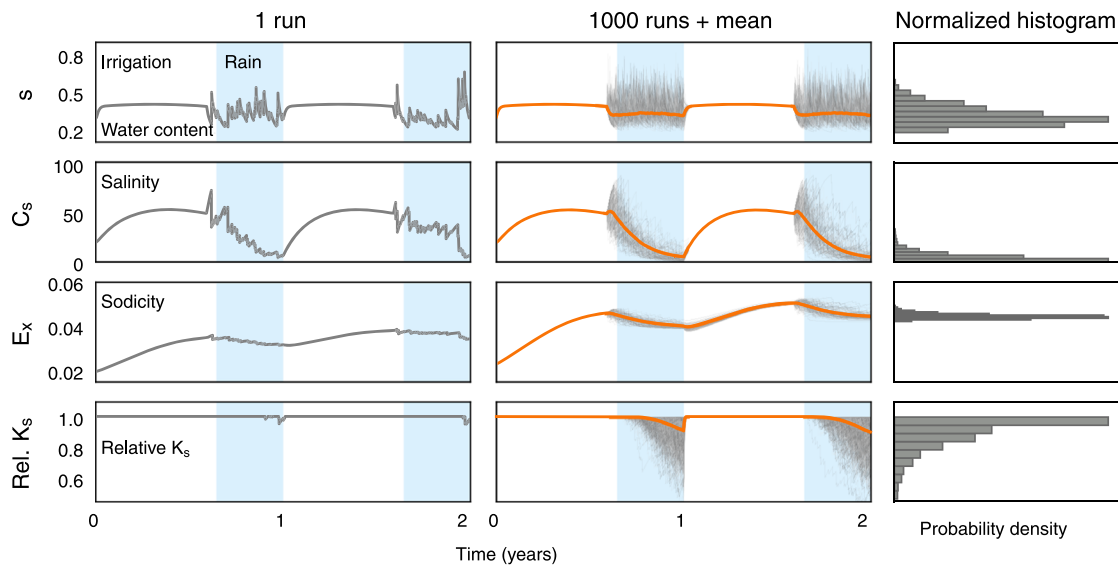
Figure 5. Example showing how stochastic ensembles are used to study the effects of climate and irrigation patterns on soils. Time series (left and middle columns) show evolution of s, C_s, E_x, and K_s. Normalized histograms (right) are based on values at conclusion of the 2-year simulation period. Simulations used Class II soil parameters; 130-day rainy season with $\lambda = 0.3$ (day^{-1}) and $\alpha = 10$ mm (390 mm/year); $I = 1.1 \cdot ET_{\max}$; $C_i = 20$ mmol$_c$/L and $E_i = 0.35$ (SAR = 2.8); and $ET_{\max}$ sinusoidal with minimum and maximum of 2 and 7 mm/day, respectively. Initial values: $s = 0.3$, $C_s = 20.0$ mmol$_c$/L, and $E_x = 0.02$.

included constant irrigation during the dry portion of the year, applied at a rate proportional to the maximum evapotranspiration rate, $I = 1.1 \cdot ET_{\max}$ (Ben-Gal & Shani, 2002; Ben-Gal et al., 2009). To account for seasonal changes in evapotranspiration rates, $ET_{\max}$ was based on a sinusoidal curve over an annual period. The minimum value in the curve was made to coincide with the midpoint of the rainy season. For simplicity, we do not consider the role of plant salt uptake or groundwater in our simulations. Parameters related to soil hydraulic properties and response of soil structure to saline and sodic conditions for the three soil types used in our simulations—Class I, Class II, and Class III—are given in Tables S1 and S2, respectively.

To demonstrate how the results in the upcoming sections are produced, we first analyze, in Figure 5, an example stochastic ensemble. The left column shows changes in relative soil water content (s), soil salinity (C_s), soil sodicity (E_x), and relative saturated hydraulic conductivity (K_s) for a single 2-year run. The center column shows 1,000 runs (thin gray lines), all using the same initial conditions, and the ensemble average of these runs (thick orange lines). The right column shows a normalized histogram (probability density) of the 1,000 run ensemble, based on the values at the conclusion of the 2 years. Focusing first on the center column, we see that the stochastic nature of the precipitation leads to variations in each of the variables during the rainy season (blue shading). The trajectories quickly converge, however, during the irrigation season (no shading). During the dry season, the input of saline and sodic irrigation water causes a rise in C_s and E_x. Leaching during the rainy season causes a decline in C_s, with values at the end of the rainy season approaching 0 mmol$_c$/L. Seasonal changes in the value of E_x are much slower and smaller in magnitude. As C_s declines and E_x remains elevated, a decline in relative K_s can be observed in a fraction of these example runs.

By studying the distribution of relative K_s at the conclusion of the example ensemble, we introduce a method for assessing the specific risk of soil degradation. No clear standard exists for defining the point at which dispersion of soil aggregates, and thereby, a significant decrease in soil permeability is likely to occur. McNeal and Coleman (1966) defined 25% reductions in relative K_s as a critical threshold, while Quirk and Schofield (1955) used 10% to 15%. We define K_{CT}, the critical threshold beyond which reductions in K_s have the potential to seriously limit water flow, to be a 20% reduction in the soil's initial saturated hydraulic conductivity. Returning to our example simulation, Figure 6a shows the probability density function (PDF) for relative hydraulic conductivity at the conclusion of the runs. Figure 6b uses these same values to compute the cumulative distribution function (CDF), which is simply the integral of the PDF. Both the PDF and CDF can be used to analyze the probability that the final relative K_s value is below K_{CT}. In what follows, we refer to the probability of the final relative K_s being less than K_{CT} as the risk of critical soil degradation. In our
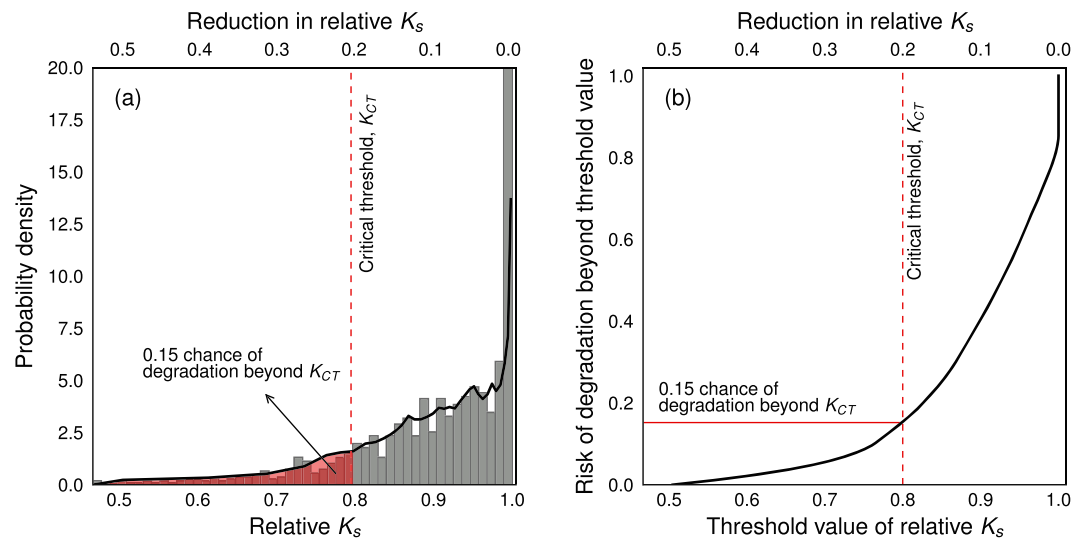
Figure 6. The risk of soil degradation can be quantified by studying the distribution of the relative K_s values. (a) Probability density function based on values at the end of the example stochastic ensemble shown in Figure 5. (b) Cumulative distribution function based on same values.

example simulation, 0.15 of the runs concluded with final relative K_s values less than K_{CT}. That is, the risk of critical soil degradation was 0.15 for this simulation.

4.2. Effect of Climate Change

Over the course of the next century, climate models forecast significant changes in seasonal rainfall patterns (Stocker, 2014). In Israel, the winter (rainy) season is expected to shorten by as much as 50% (Dubrovsky et al., 2014; Hochman et al., 2018). To examine how a shorter rainy season might affect the risk of soil degradation, we compared simulations using the current climate in Israel's Northern Negev region (130-day rainy season) to simulations with an 80-day winter. To reflect the possibility that extreme rainfall events may become more likely as winters shorten (Dubrovsky et al., 2014), we made the mean event height inversely proportional to the length of the winter, while holding the total annual rainfall constant.

When designing our simulations, we also considered how irreversible changes in soil hydraulic conductivity may affect soil degradation. Existing models for the effect of salinity and sodicity on K_s, including the Ezlit et al. (2013) model, consider soil degradation and rehabilitation to be reversible processes. That is, while changes to soil salinity and sodicity can cause K_s to decline, if the changes to salinity and sodicity are reversed, then K_s will immediately return to its original value. The scant experimental evidence that exists, however, suggests that these processes feature hysteresis, that is, the system follows different paths for degradation and rehabilitation (Dane & Klute, 1977). To probe how this hysteresis may influence our risk assessment, we executed an additional set of simulations, in which SOTE was modified as follows: If the value of K_s fell below 80% of its initial value (i.e., degraded beyond K_{CT}) then the value of K_s thereafter could only decrease. In cases where K_s declined, but remained above K_{CT}, we continued to treat degradation as reversible.

The ensemble averages for our state variables (s, C_s, E_x) and relative K_s during the simulation period are presented in Figure 7. Figure 7 also includes PDFs based on the values of these variables at the conclusion of the 20-year-long simulation. The dashed lines correspond to the simulations in which reductions in K_s beyond K_{CT} were treated as irreversible. Consideration of irreversible degradation only affected the shorter rainy season and therefore there are no dashed lines associated with the 130-day winter.

The difference in rainy season length causes clear changes in annual salt leaching from the soils. Under the 130-day rainfall regime, C_s declines during each rainy season, but the soil is incompletely leached. In general, areas receiving less than 500 mm of rain per year are susceptible to long-term salt accumulation unless the soil is properly leached with irrigation water (Lado et al., 2012). Given that the annual rainfall in our simulation is 214 mm and that our irrigation water is saline, lack of complete leaching is not surprising.
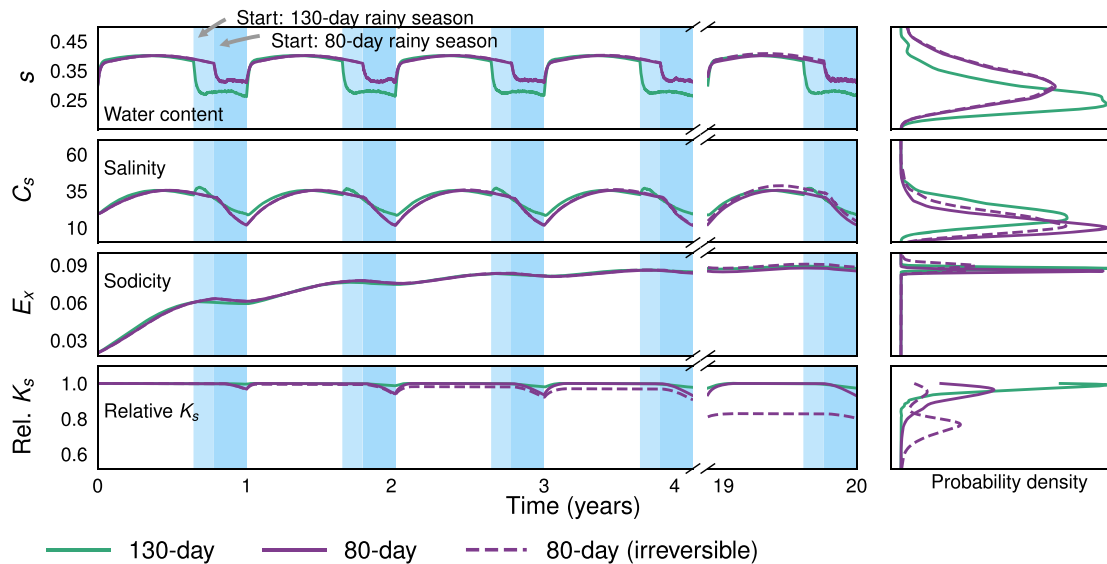
Figure 7. A shorter rainy season increases leaching in C_s, making soils more susceptible to degradation in hydraulic conductivity. Consideration of irreversibility significantly affects the likelihood of degradation. Time series (left) show ensemble averages for changes in s, C_s, E_x, and K_s, based on 1,000 runs for 20 years. PDFs (right) estimated from values at the end of the simulation period. Simulations run using 130-day ($\alpha = 5.5$ mm) and 80-day ($\alpha = 8.125$ mm) rainy seasons and $\lambda = 0.3$ (day^{-1}) (annual rainfall of 214 mm). Irrigation water properties: $C_i = 10$ mmol$_c$/L and $E_i = 0.55$ (SAR = 3.7). Other properties as defined in Figure 5.

When the rainfall occurs over only an 80-day season, however, leaching of salts is increased and C_s reaches a lower level at the end of the annual rainy season.

The increased leaching of salts during the shorter rainy season results in a greater risk of soil degradation. The risk of degradation in hydraulic conductivity increases during the shorter rainy season because, in contrast to the C_s values, E_x hardly declines during the shorter rainy season. This difference results from changes to C_s occurring on much faster time scales than changes in E_x (Mau & Porporato, 2015).

The increased risk of soil degradation is even larger when irreversible conditions are considered. The CDF emphasizes the increased risk of degradation during the shorter winter, particularly when irreversible changes are possible. Figure 8 shows that the risk of critical soil degradation was 0.0 in the 130-day winter and 0.03 in the 80-day winter, when degradation was treated as reversible. When irreversible degradation was considered, however, the risk of critical degradation rose to 0.68. When degradation and rehabilitation are treated as reversible, declines in hydraulic conductivity during the rainy season are reversed during the dry season, when saline irrigation water is applied. When irreversible changes are possible, however, the hydraulic conductivity of a fraction of the runs remains degraded even when irrigated with saline water. This difference is particularly visible in year 20 of the simulations, when the ensemble average of the hydraulic conductivity is significantly lower for the irreversible 80-day rainy season (Figure 7). We implemented a crude mechanism for the potential effect of irreversible degradation: After K_s fell below 80% of its initial value, future rises were precluded. The great increase in degradation risk, from 3% to 68%, underscores the need to better account for partial reversibility in K_s degradation, which is, however, out of the scope of this paper.

4.3. Effect of Irrigation Water and Soil Type

In many parts of the world, especially in arid and semiarid regions, rising human populations are increasing stress on limited water resources. At the same time, growing human populations are augmenting pressure on agricultural systems to meet food demands—encouraging irrigation with low-quality water and farming on marginal lands. SOTE can help us understand how irrigation practices, together with the climate and soil type in the farmed area, may affect soil degradation. In this respect, SOTE can help planners determine which type of irrigation water quality will minimize the risk of long-term land degradation, given a particular soil type and climate.
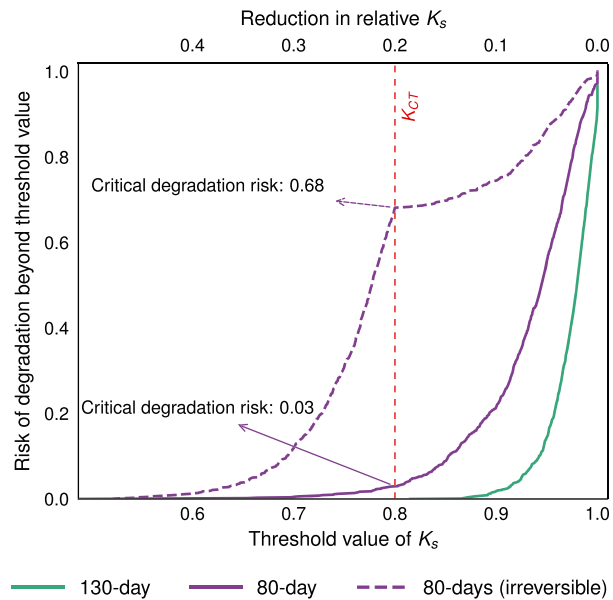
Figure 8. CDF shows a shorter rainy season may increase the risk of soil degradation in arid and semiarid regions. Simulations properties as defined in Figure 7.

4.3.1. Chemical Composition of Irrigation Water

To demonstrate how irrigation with low-quality water may increase the risk of soil degradation, we conducted simulations with irrigation water of three different chemical compositions: fresh water, treated waste water, and brackish water. The salinity and sodicity fraction of the respective irrigation waters were based on values reported in Mantell et al. (1985) and Levy et al. (2014). The salinity ranged from 12 mmol$_c$/L in the fresh water to 20 and 35 mmol$_c$/L in the treated waste water and brackish water, respectively. The simulations used an SAR of 1.1 for the fresh water, 2.7 for the treated waste water, and 5.9 for the brackish water. The ensemble averages for our state variables (s, C_s, E_x) and relative K_s during the simulation period show that the different irrigation waters lead to clear differences in soil salinity and sodicity (Figure 9). Not
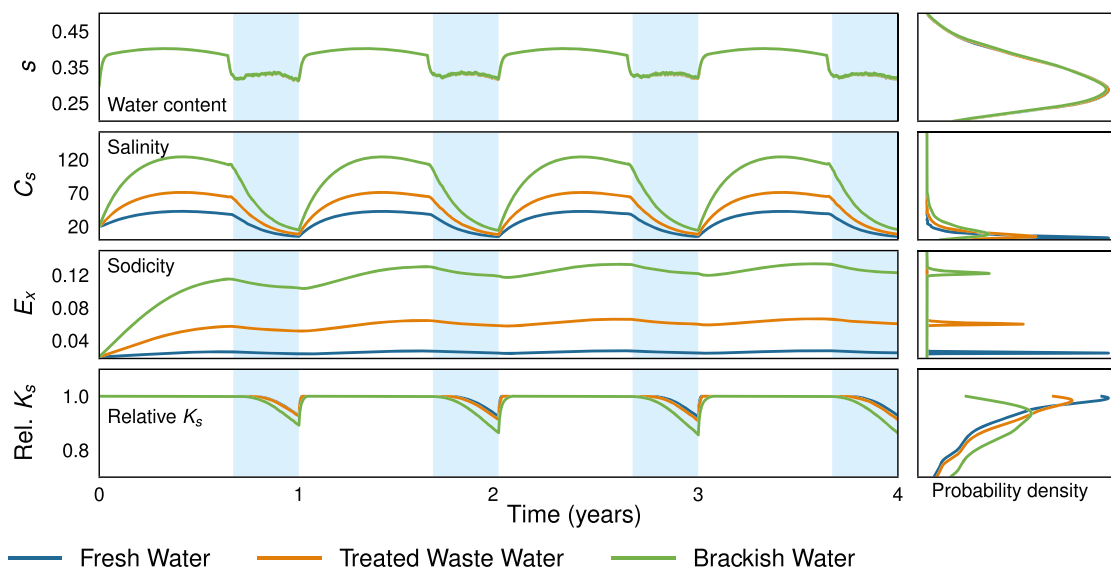

Figure 9. Time series (left) show that application of low-quality irrigation water leads to higher soil sodicity, increasing the risk of degradation when salinity declines during rainy season. PDFs (right) computed from values at the end of the simulation period. Simulations run using three water qualities. (i) Fresh water: $C_i = 12\,\text{mmol}_c/\text{L}$, $E_i = 0.2$, SAR = 1.1. (ii) Treated waste water: $C_i = 20\,\text{mmol}_c/\text{L}$, $E_i = 0.35$, SAR = 2.7. (iii) Brackish water: $C_i = 35$ mmol$_c$/L, $E_i = 0.5$, SAR = 5.9. Other properties as defined in Figure 5.
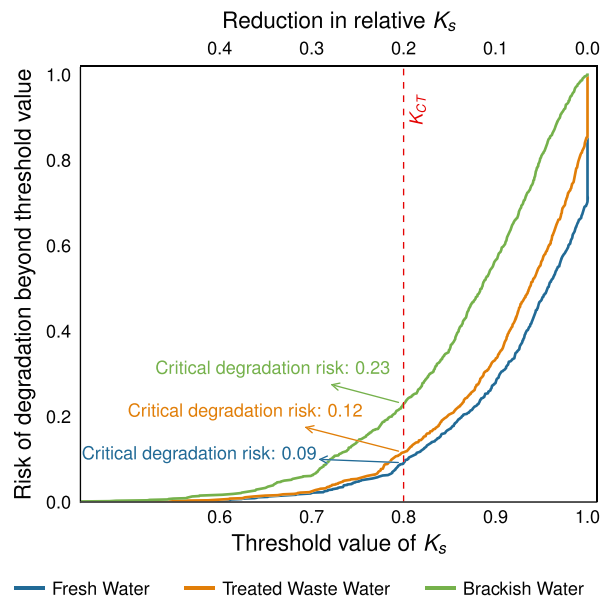
Figure 10. CDF shows irrigation with low-quality water has the potential to raise degradation risks. Simulation properties as defined in Figure 9.

surprisingly, irrigation with brackish water, the most saline and sodic of the three waters, leads to the highest levels of soil salinity and sodicity.

The high levels of salinity and sodicity resulting from the application of brackish irrigation water increase the risk of soil degradation. As seen in section 4.2, large declines in C_s are possible during the rainy season, while E_x changes on a much slower scale. In particular, irrigation with brackish water raises the salinity and sodicity of the soil, but during the rainy season only the salinity declines, leaving the soil vulnerable to declines in relative K_s. Figure 10 presents the CDF for each of the irrigation waters. The risk of critical degradation in the soil irrigated with fresh water and treated waste water is 0.09 and 0.12, respectively. With brackish water, however, the risk is nearly double, rising to 0.23. The results presented here do not consider the possibility of irreversible degradation, but as shown in the preceding section, consideration of irreversible degradation has the potential to exacerbate the risk posed by seasonal degradation cycles. This will be the subject of forthcoming research, investigating how irreversible degradation processes compound the risk presented by sodic irrigation water.

Our results emphasize the need to carefully consider how a particular irrigation water quality will affect the specific soil to which it is applied. While outside the scope of this paper, extending the principles developed in these simulations would allow us to explore the nonlinear interplay between irrigation regimes, soil texture, water quality, and degradation risk. This issue is especially important because utilization of marginal quality water and lands can help alleviate some of the expected pressure on water resources and food supplies, but this advantage will be sacrificed if more land is lost to degradation.

4.3.2. Clay Content of Soil

The effect of a particular irrigation regime depends on the properties of the soil to which it is applied. To examine how soil type may contribute to degradation risks, we studied three soils, each with different clay contents, under the same climate and irrigation regime. Figure 11 presents the ensemble averages for our state variables (s, C_s, E_x) and relative K_s during the simulation period. The time series show clear differences between the salinity and sodicity dynamics of the Class I (5.7% clay), Class II (16.2% clay), and Class III (48.5% clay) soils. The Class I and Class II soils behave similarly. They experience increases in C_s during the dry season, when irrigation is applied, and declines during rainy season, as a result of salt leaching. Initially, E_x rises in these two soils due to the application of saline and sodic irrigation water. Following the initial rise, however, the value of E_x remains relatively stable, experiencing small declines each rainy season and small rises when irrigation water is applied. In the Class III soil, however, C_s reaches much higher levels and actually continues to rise during the rainy season. Likewise, the value of E_x in the Class III soil is higher than in the other soils. These contrasting patterns result from differences in the hydraulic properties of the soils. The
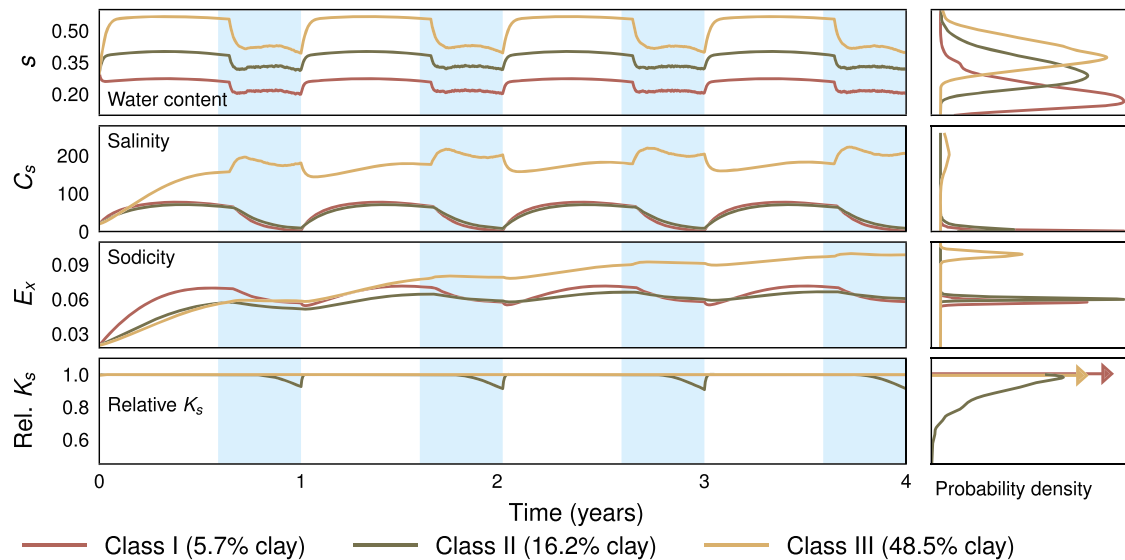
Figure 11. Higher clay content, associated with higher susceptibility to degradation, does not necessarily translate to higher degradation risk. Panels on the left show the dynamics of state variables s, C_s, E_x, and relative K_s over a period of four years. Panels on the right show the spread for each variable at the end of simulation period. Arrows in the bottom left panel indicate that Class I and Class III have no spread in K_s. Simulation properties as defined in Figure 5.

Class III soil, which is highest in clay content, has a much lower hydraulic conductivity and by extension drains at a much slower rate than the other soils. Because leaching is the primary method through which salts can leave the soil, the significantly lower leaching rate in the Class III soil leads to the long-term accumulation of salts. The CDF for this set of simulations is included in the supporting information (Figure S5), while we note here that the probability of critical degradation in the Class II soil was 0.12.

Although the Class III soil is highest in clay content, it does not experience any degradation. The high salinity observed in the the Class III soil, while itself a significant hurdle to agricultural production, also acts as a barrier to sodicity-related degradation. As shown in Figure 2, the higher the salt concentration, the more resilient the soil will be to reductions in K_s at a given sodicity level. Meanwhile, even though the salinity and sodicity dynamics in the Class I and Class II soils are similar, only the Class II soil experiences degradation in K_s. The results here underscore the need to take an integrated approach when assessing degradation risks—one that considers the interplay between the fundamental feedbacks in the soil (in our case the exchange reaction and the reduction in K_s) and the stochastic drivers of the system (rainfall). These results also emphasize the importance of integrating models that consider soil-specific properties, such as the Ezlit et al. (2013) model, when assessing degradation risks. Incorporating the Ezlit et al. (2013) model into dynamical models for salinity and sodicity, such as SOTE, gives us the potential not only to examine how the relative clay content influences degradation risk but also to account for differences between clay types. Finally, there is an important distinction to be made between susceptibility and risk, since higher clay contents do not always translate to a higher risk of degradation.

5. Discussion and Conclusions

We presented here a tool for assessing long-term soil degradation risks associated with salinization and sodification. The SOTE model focuses on two major processes related to the dynamics of salt in the soil. The first is the exchange reaction between cations in the soil solution and the exchange complex. The second feedback is the dependence of the saturated hydraulic conductivity on salinity/sodicity levels. These two processes successfully manage to account for the long-term dynamics of water and salt in the root zone. SOTE's suitability for studying long-term degradation risks comes from its focus, simplicity, and ease of use. The mechanisms and equations underlying SOTE are relatively simple, making the execution of thousands of simulations, covering long periods of time, computationally efficient. Because of this, SOTE is more amenable than existing models, both complex and simple, to large-ensemble simulations of stochastic climatic conditions, for which trends in the statistics of salinization and soil degradation can be identified. In this paper, we considered only one type of irrigation regime and did not consider interannual variability

in rainfall patterns. Due to this simplicity, the dynamics in soil water content, salinity, and sodicity were observed to stabilize within a relatively short time period. Future research, however, should consider different irrigation regimes and interannual variations in rainfall, which will lead to richer dynamics, for which SOTE's ability to handle long-term simulations is well suited. Of course, while the SOTE model can point to the risk of soil degradation, our results also demonstrate the need for additional experimental work be conducted, using a range of soil types and covering long-term time periods. Such experiments will allow further evaluation of SOTE's predictive power and increase our understanding of the effects of marginal quality waters on soils.

While SOTE is simple on the one hand, it is also explicitly focused on the dynamics that drive degradation and incorporates the soil-specific Ezlit et al. (2013) model for the effect of salinity and sodicity on hydraulic conductivity. Together, this combination makes SOTE a novel tool for assessing the risk of soil degradation resulting from different irrigation water qualities and climate regimes. Most existing models for the dynamics of salinity and sodicity, by contrast, are not capable of considering the effect of soil type on changes to hydraulic conductivity. While the advantages of a soil-specific approach have been demonstrated, the incorporation of soil-specific considerations into existing models for the dynamics of salinity and sodicity has been hampered, possibly due to difficulties in modifying the code of these existing models (Ali et al., 2019; van de Craats et al., 2020). As an open-source program coded in Python, SOTE is easily amenable to user modifications. Furthermore, SOTE's interface is accessible with minimal user training and because SOTE focuses only on salinity and sodicity, its use is not predicated on familiarity with numerous exterior soil processes.

There is a trade-off between a model's simplicity and its precision. While the advantages of precision are clear, simple models are an asset for analysis and for identifying patterns in the main processes being studied. In this paper, for example, we took advantage of SOTE's simplicity to show that shorter rainy seasons will increase degradation risk. We also showed that the soil with the greatest clay content is not necessarily the one that will undergo deterioration. In focusing on a small number of basic processes, we left aside other phenomena that can be incorporated into SOTE. More refined infiltration descriptions that consider how rainfall intensity may affect the upper layer of the soil profile could, for instance, be easily incorporated into SOTE. Likewise, SOTE could be modified to include more detailed chemistry, coupled plant dynamics, or a layered soil profile.

In this paper, we also demonstrated how consideration of irreversibility in K_s radically altered the probability of degradation in our simulations. A better account of the partial reversibility of K_s must be developed and incorporated to all models if we are to accurately assess long-term degradation risks.

Data Availability Statement

For the validation section of our manuscript, we relied on data from Gonçalves et al. (2006), which was provided to us upon request. We are sincerely grateful to Maria da Conceição Gonçalves for her assistance with this data. Results from the validation of SOTE, including the measured results and Hydrus results to which SOTE was compared, are available online in our Zenodo repository: https://doi.org/10.5281/zenodo.3928221. We encourage readers to download and use the Python code implementation of SOTE, which is hosted on Github. The repository also contains a description of the parameters related to soil properties, as described in the manuscript itself. A link to the GitHub repository is available online (https://github.com/isaackramer/SOTE).

References

Ahuja, L., Rojas, K. W., & Hanson, J. D. (2000). *Root zone water quality model: Modelling management effects on water quality and crop production.* Highlands Ranch, CO USA: Water Resources Publication.

Ali, A., Biggs, A. J. W., Marchuk, A., & Bennett, J. M. (2019). Effect of irrigation water pH on saturated hydraulic conductivity and electrokinetic properties of acidic, neutral, and alkaline soils. *Soil Science Society of America Journal*, *83*(6), 1672–1682.

Ben-Gal, A., Agam, N., Alchanatis, V., Cohen, Y., Yermiyahu, U., Zipori, I., et al. (2009). Evaluating water stress in irrigated olives: Correlation of soil water status, tree water status, and thermal imagery. *Irrigation Science*, *27*(5), 367–376.

Ben-Gal, A., & Shani, U. (2002). Yield, transpiration and growth of tomatoes under combined excess boron and salinity stress. *Plant and soil*, *247*(2), 211–221.

Chesworth, W. (Ed.) (2008). *Encyclopedia of soil science Edited by* Chesworth, W. Dordrecht, The Netherlands: Springer.

Clapp, R. B., & Hornberger, G. M. (1978). Empirical equations for some soil hydraulic properties. *Water Resources Research*, *14*(4), 601–604.

Dane, J. H., & Klute, A. (1977). Salt effects on the hydraulic properties of a swelling soil 1. *Soil Science Society of America Journal*, *41*(6), 1043–1049.

Dang, A., Bennett, J. M., Marchuk, A., Marchuk, S., Biggs, A. J. W., & Raine, S. R. (2018). Validating laboratory assessment of threshold electrolyte concentration for fields irrigated with marginal quality saline-sodic water. *Agricultural Water Management*, *205*, 21–29. https://doi.org/10.1016/J.AGWAT.2018.04.037

Dubrovsky, M., Hayes, M., Duce, P., Trnka, M., Svoboda, M., & Zara, P. (2014). Multi-GCM projections of future drought and climate variability indicators for the Mediterranean region. *Regional Environmental Change*, *14*(5), 1907–1919.

El-Din, M. M. N., King, I. P., & Tanji, K. K. (1987). Salinity management model: I. Development. *Journal of Irrigation and Drainage Engineering*, *113*(4), 440–453. https://doi.org/10.1061/(ASCE)0733‐9437(1987)113:4(440)

Ezlit, Y. D., Bennett, J. M., Raine, S. R., & Smith, R. J. (2013). Modification of the McNeal clay swelling model improves prediction of saturated hydraulic conductivity as a function of applied water quality. *Soil Science Society of America Journal*, *77*(6), 2149. https://doi.org/10.2136/sssaj2013.03.0097

FAO, & ITPS (2015). *Status of the world's soil resources*. Rome, Italy: Food and Agriculture Organization of the United Nations and Intergovernmental Technical Panel on Soils.

Farthing, M. W., & Ogden, F. L. (2017). Numerical solution of Richards' equation: A review of advances and challenges. *Soil Science Society of America Journal*, *81*(6), 1257. https://doi.org/10.2136/sssaj2017.02.0058

Gonçalves, M. C., Šimůnek, J., Ramos, T. B., Martins, J. C., Neves, M. J., & Pires, F. P. (2006). Multicomponent solute transport in soil lysimeters irrigated with waters of different quality. *Water Resources Research*, *42*, W08401. https://doi.org/10.1029/2005WR004802

Hillel, D. (1998). *Environmental soil physics*. San Diego, California: Academic Press.

Hillel, D. (2000). *Salinity management for sustainable irrigation: Integrating science, environment, and economics*. Washington, DC: The World Bank.

Hochman, A., Harpaz, T., Saaroni, H., & Alpert, P. (2018). The seasons' length in 21st century CMIP5 projections over the eastern Mediterranean. *International Journal of Climatology*, *38*, 2627–2637. https://doi.org/10.1002/joc.5448

Hutson, J. L., & Wagenet, R. J. (1989). *LEACHM: Leaching estimation and chemistry model: A process-based model of water and solute movement, transformations, plant uptake and chemical reactions in the unsaturated zone; version 2*. Ithaca, NY: Cornell Univ., Center for Environmental Research.

Kroes, J. G., Van Dam, J. C., Groenendijk, P., Hendriks, R. F. A., & Jacobs, C. M. J. (2009). SWAP version 3.2. Theory description and user manual. Wageningen, The Netherlands: Alterra.

Läuchli, A., & Grattan, S. R. (2011). Plant responses to saline and sodic conditions. In W. W. Wallender, & K. K. Tanji (Eds.), *Agricultural salinity assessment and management* (pp. 169–205). Reston, VA: American Society of Civil Engineers. https://doi.org/10.1061/9780784411698.ch06

Lado, M., Bar-Tal, A., Azenkot, A., Assouline, S., Ravina, I., Erner, Y., et al. (2012). Changes in chemical properties of semiarid soils under long-term secondary treated wastewater irrigation. *Soil Science Society of America Journal*, *76*(4), 1358. https://doi.org/10.2136/sssaj2011.0230

Laio, F., Porporato, A., Ridolfi, L., & Rodriguez-Iturbe, I. (2001). Plants in water-controlled ecosystems: Active role in hydrologic processes and response to water stress: II. Probabilistic soil moisture dynamics. *Advances in Water Resources*, *24*(7), 707–723.

Levy, G. J., Fine, P., Goldstein, D., Azenkot, A., Zilberman, A., Chazan, A., & Grinhut, T. (2014). Long term irrigation with treated wastewater (TWW) and soil sodification. *Biosystems Engineering*, *128*, 4–10. https://doi.org/10.1016/j.biosystemseng.2014.05.004

Mantell, A., Frenkel, H., & Meiri, A. (1985). Drip irrigation of cotton with saline-sodic water. *Irrigation Science*, *6*(2), 95–106.

Mau, Y., Feng, X., & Porporato, A. (2014). Multiplicative jump processes and applications to leaching of salt and contaminants in the soil. *Physical Review E*, *90*(5), 052128. https://doi.org/10.1103/physreve.90.052128

Mau, Y., & Porporato, A. (2015). A dynamical system approach to soil salinity and sodicity. *Advances in Water Resources*, *83*, 68–76. https://doi.org/10.1016/j.advwatres.2015.05.010

Mau, Y., & Porporato, A. (2016). Optimal control solutions to sodic soil reclamation. *Advances in Water Resources*, *91*, 37–45. https://doi.org/10.1016/j.advwatres.2016.02.014

McNeal, B. L. (1968). Prediction of the effect of mixed-salt solutions on soil hydraulic conductivity. *Soil Science Society of America Journal*, *32*, 190–193. https://doi.org/10.2136/sssaj1968.03615995003200020013x

McNeal, B. L., & Coleman, N. T. (1966). Effect of solution composition on soil hydraulic conductivity. *Soil Science Society of America Journal*, *30*(3), 308–312. https://doi.org/10.2136/sssaj1966.03615995003000030007x

Perri, S., Suweis, S., Entekhabi, D., & Molini, A. (2018). Vegetation controls on dryland salinity. *Geophysical Research Letters*, *45*, 11,669–11,682. https://doi.org/10.1029/2018GL079766

Quirk, J. P., & Schofield, R. K. (1955). The effect of electrolyte concentration on soil permeability. *Journal of Soil Science*, *6*(2), 163–178. https://doi.org/10.1111/j.1365‐2389.1955.tb00841.x

Raveh, E., & Ben-Gal, A. (2016). Irrigation with water containing salts: Evidence from a macro-data national case study in Israel. *Agricultural Water Management*, *170*, 176–179. https://doi.org/10.1016/j.agwat.2015.10.035

Rodriguez-Iturbe, I., & Porporato, A. (Eds.). (2004). *Ecohydrology of water-controlled ecosystems: Soil moisture and plant dynamics*. Cambridge, UK: Cambridge University Press. https://doi.org/10.1017/CBO9780511535727

Russo, D. (1989). Field-scale transport of interacting solutes through the unsaturated zone: 2. Analysis of the spatial variability of the field response. *Water Resources Research*, *25*(12), 2487–2495.

Shah, S. H. H., Vervoort, R. W., Suweis, S., Guswa, A. J., Rinaldo, A., & Van Der Zee, S. E. A. T. M. (2011). Stochastic modeling of salt accumulation in the root zone due to capillary flux from brackish groundwater. *Water Resources Research*, *47*, W09506. https://doi.org/10.1029/2010WR009790

Short, D., Dawes, W. R., & White, I. (1995). The practicability of using Richards' equation for general purpose soil-water dynamics models. *Environment International*, *21*(5), 723–730. https://doi.org/10.1016/0160-4120(95)00065-S

Stocker, T. (2014). *Climate change 2013: The physical science basis: Working Group I contribution to the Fifth assessment report of the Intergovernmental Panel on Climate Change*. New York, NY: Cambridge University Press.

Suweis, S., Rinaldo, A., van der Zee, S. E. A. T. M., Daly, E., Maritan, A., & Porporato, A. (2010). Stochastic modeling of soil salinity. *Geophysical Research Letters*, *37*, L07404. https://doi.org/10.1029/2010GL042495

Tanji, K. K., & Deverel, S. J. (1984). Reclamation of sodic soils. In I. Shainberg, & S. J. Deverel (Eds.), *Soil salinity under irrigation* (pp. 220–257). Berlin, Germany: Springer Berlin Heidelberg. https://doi.org/10.1007/978-3-642-69836-1_7

The Water Resources Group (2012). Background, impact and the way forward. Davos-Klosters, Switzerland: World Economic Forum.

Tocci, M. D., Kelley, C. T., & Miller, C. T. (1997). Accurate and economical solution of the pressure-head form of Richards' equation by the method of lines. *Advances in Water Resources*, *20*(1), 1–14. https://doi.org/10.1016/S0309-1708(96)00008-5

van de Craats, D., van der Zee, S. E. A. T. M., Sui, C., van Asten, P. J. A., Cornelissen, P., & Leijnse, A. (2020). Soil sodicity originating from marginal groundwater. *Vadose Zone Journal*, *19*(1), e20010.

van der Zee, S. E. A. T. M., Shah, S. H. H., van Uffelen, C. G. R., Raats, P. A. C., & dal Ferro, N. (2010). Soil sodicity as a result of periodical drought. *Agricultural Water Management*, *97*, 41–49. https://doi.org/10.1016/j.agwat.2009.08.009

van der Zee, S. E. A. T. M., Shah, S. H. H., & Vervoort, R. W. (2014). Root zone salinity and sodicity under seasonal rainfall due to feedback of decreasing hydraulic conductivity. *Water Resources Research*, *50*, 9432–9446. https://doi.org/10.1002/2013WR015208

Vereecken, H., Schnepf, A., Hopmans, J. W., Javaux, M., Or, D., Roose, T., et al. (2016). Modeling soil processes: Review, key challenges, and new perspectives. *Vadose Zone Journal*, *15*(5), 1–57. https://doi.org/10.2136/vzj2015.09.0131

Vervoort, R. W., & van der Zee, S. E. A. T. M. (2008). Simulating the effect of capillary flux on the soil water balance in a stochastic ecohydrological framework. *Water Resources Research*, *44*, W08425. https://doi.org/10.1029/2008WR006889

Vico, G., & Porporato, A. (2010). Traditional and microirrigation with stochastic soil moisture. *Water Resources Research*, *46*, W03509. https://doi.org/10.1029/2009WR008130

Wallender, W. W., & Tanji, K. K. (Eds.). (2011). *Agricultural salinity assessment and management* (2nd ed.). Reston, VA: American Society of Civil Engineers. https://doi.org/10.1061/9780784411698

Šimůnek, J., Sakai, M., Van Genuchten, M., Saito, H., & Sejna, M. (2013). The HYDRUS-1D software package for simulating the one-dimensional movement of water, heat, and multiple solutes in variably-saturated media. Riverside, CA 92521, USA: University of California, Riverside.

Šimůnek, J., & Suarez, D. L. (1997). Sodic soil reclamation using multicomponent transport modeling. *Journal of Irrigation and Drainage Engineering*, *123*(5), 367–376. https://doi.org/10.1061/(ASCE)0733-9437(1997)123:5(367)